ACS Sustainable Chemistry & Engineering

Research Article

pubs.acs.org/journal/ascecg

Producing Hydrogen-Rich Gases by Steam Reforming of Syngas Tar over CaO/MgO/NiO Catalysts

Ali A. Rownaghi* and Raymond L. Huhnke

Biosystems and Agricultural Engineering, Oklahoma State University, Stillwater, Oklahoma 74078, United States

ABSTRACT: The objective of this study was to develop nanosized CaO, MgO, and NiO catalysts for tar removal in biomass gasification, significantly enhancing the quality of the produced gases. Catalysts were tested in a fixed-bed reactor for biomass tar steam reforming. Toluene was chosen as a model syngas tar compound. For this purpose, pure $Ca(OH)_2$, $Mg(OH)_2$, and $Ni(OH)_2$ precursors were successfully synthesized via a facile solvothermal method. Subsequent calcination of the metal hydroxide precursor at 450 °C resulted in nanosized CaO, MgO, and NiO. Different analytical techniques such as XRD, TEM, SEM, and BET were used to characterize the synthesized nanomaterials. Bulk NiO, CaO, and MgO nanomaterials and a physical mixture of CaO/MgO/NiO (equal NiO/CaO/MgO ratio) were used as catalysts for the steam gasification of toluene. Research showed higher toluene conversions, which resulted in increases in H_2 yield as well as CO and CO_2 selectivity. Mixed metal oxide CaO/MgO/NiO catalyst exhibited higher performance on toluene conversion, resulting in higher H_2 yield and CO_2 selectivity.

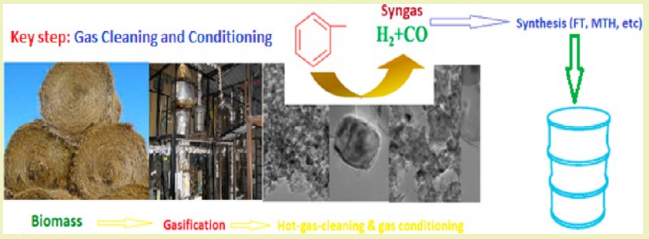

KEYWORDS: *Biomass gasification, Gas cleaning and conditioning, Mixed metal oxide catalysts*

INTRODUCTION

In the 21 century, biomass is perceived as an attractive source of biofuels and chemicals.[1−6] Thermochemical gasification of biomass is one of the promising routes of using this abundantly available and highly diverse renewable energy source.[7] The raw gasification product gas contains CO, CO_2, H_2, CH_4, H_2O, and N_2 as main constituents. However, in addition to these main gas components, the gas contains organic and inorganic impurities and particulates.[4,7]Therefore, the removal of organic (light hydrocarbons and tar) and inorganic (nitrogen-, sulfur-, and chlorine-containing contaminants, i.e., NH_3, HCN, H_2S, HCl, and alkali metal) impurities from the syngas is required.[8−14] In this study, tar is the primary focus. Tar is a complex mixture of condensable hydrocarbons, which includes single-ring to polycyclic aromatic hydrocarbons (PAHs) compounds along with other oxygen-containing hydrocarbons and complex.[11] Tars can present a number of process challenges, including coking of catalysts and condensation on downstream piping, filters, and other equipment.[13] The cost of tar removal can be as much as the overall process cost to produce the biofuel.[14]

Gas cleaning and conditioning are currently among the major areas of study in the field of biomass gasification. The main techniques involved in gas cleaning are physical, mechanical, granular beds, catalytic, and thermal cracking methods. The hot gas cleanup is a more preferable technology because energy loss is minimized by avoiding cooling of raw product gas.[9,10] Catalytic tar removal has received much attention because tars can be cracked or reformed into gaseous components, increasing the overall efficiency of the gasification process. Many types of heterogeneous catalysts have been studied intensively as alternative catalysts for tar elimination, for example, olivine, clay minerals, ferrous metal oxides, char, zeolites, alkaline, alkaline earth, activated alumina, and transition-metal-based catalysts, particularly nickel (Ni).[11−13] The most widely researched catalysts have been dolomites, alkali metals, and nickel. Ngamcharussrivichai et al. claimed that a natural Ca−Mg mixed carbonate termed "dolomite" was the source material appropriate to the preparation of the active CaMgO catalyst.[15,16] Dolomite, which has low toxicity, is a very abundant material in the world. Comprising alternating layers of $Mg(CO_3)$−$Ca(CO_3)$, natural sources may also contain Ca-rich phases of magnesium calcite ($Mg_xCa_{1-x}CO_3$). Upon the calcination of dolomite, MgO grows on the surface of $MgCa(CO_3)_2$, which is progressively transformed into $CaCO_3$ followed by the decomposition of calcite to CaO.[8] The catalytic performance of dolomite in tar cracking is directly proportional to the number of surface base sites.[13] Several approaches for tar reduction have been reported.[11−14] A major part of ongoing research deals with the development of efficient methods for tar removal in an economical and optimized way. Ni/olivine, Ni/dolomite, and Ni/Al_2O_3 have been applied extensively for biomass gasification tar conversion because nickel-based catalysts are very active for tar abatement.[14,17] Because of their catalytic properties, NiO particles have attracted much attention for their catalytic properties. In recent years, nanomaterials have attracted extensive attention for their unique properties in various fields in comparison with their

Received: July 11, 2012
Revised: November 3, 2012
Published: November 12, 2012

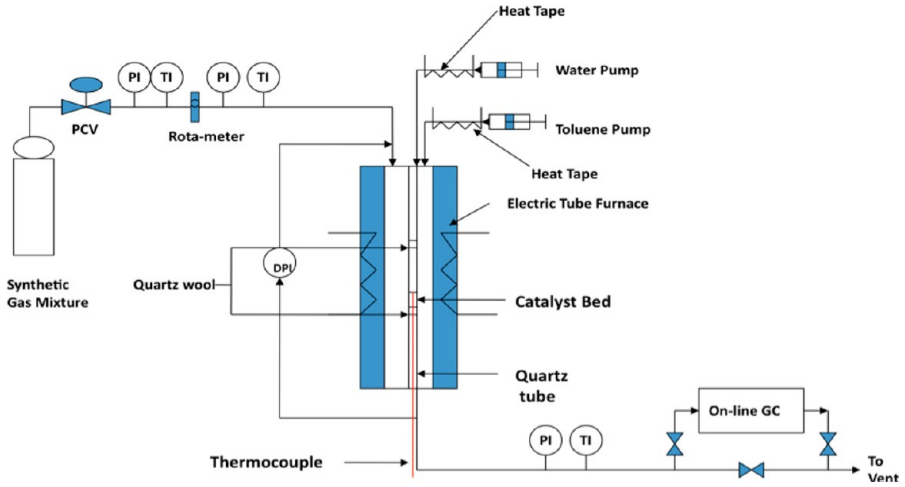

Figure 1. Schematic diagram of the experimental apparatus (fixed-bed reactor).

bulk counterparts.[18] Nanosized NiO particles can be loaded on the surface of distinct carriers (such as dolomite and olivine) to prepare the supported catalyst.[14,17] Unfortunately, not all of the aforementioned catalysts have been extensively studied. Therefore, it is necessary to identify effective catalysts with high tar conversion and resistance to coke deactivation.

Recently, Rownaghi et al.[19−21] successfully synthesized vanadium oxide nanocrystallines through a very simple solvothermal technique. Further studies demonstrated that the structure, crystallite size, and surface morphology of the obtained nanocrystals can be controlled by this method.[19−21] The objective of this study was to develop a novel and low-cost method to synthesis nanosized MgO, CaO, and NiO catalysts to break down toluene, a model tar compound for tar removal in biomass gasification.

All nanocrystalline from the calcination of thus-prepared $Mg(OH)_2$, $Ca(OH)_2$, and $Ni(OH)_2$ precursors were also investigated by a series of characterization techniques. We found the obtained MgO, CaO, and NiO did show a high surface area feature. Following that, catalytic activities of the prepared catalysts were evaluated for elimination of toluene as the tar model compound in a bench-scale fixed-bed reactor by using the bulk of CaO, MgO, and NiO catalysts and mixed metal oxide with equal Ca/Mg/Ni atomic ratio.

EXPERIMENTAL SECTION

Catalyst Preparation. $Ca(OH)_2$, $Mg(OH)_2$, and $Ni(OH)_2$ precursors were prepared by the solvothermal method using $Ca(NO_3)_2{\cdot}6H_2O$, $Mg(NO_3)_2{\cdot}6H_2O$, and $Ni(NO_3)_2{\cdot}6H_2O$ as metal sources and methanol−toluene as the reactants. All reagents were analytical-grade pure (Sigma-Aldrich). In a solvothermal procedure, 0.08 mol of the hydroxide gel solution was transferred into a Teflon-lined autoclave of 125 mL capacity. Then the autoclave was filled with aqueous ammonia solution up to 2/3 of the total volume. The autoclave was sealed and placed in an oven and maintained at 180 °C for 24 h. After cooling the autoclave to room temperature naturally, the $Ca(OH)_2$, $Mg(OH)_2$, and $Ni(OH)_2$ precursors were purified by repeated centrifugation (2700 rpm for 30 min) followed by redispersion in distilled water for four times in total. The purified product was dried in a vacuum at 60 °C for 16 h. At this stage of preparation, the sample was mostly in the hydroxide form. All metal precursors were subsequently calcined in air in a muffle furnace using a programmed temperature profile. The temperature was increased very slowly (2 °C/min) to avoid the sudden collapse of the structure. When the samples reached an ambient temperature of 250 °C, this condition was held for 2 h. The process was then continued to 350 °C and held for 2 h, and finally increased to 450 °C and held at this temperature for 4 h.

Catalyst Characterizations. X-ray powder diffraction (XRD) patterns were recorded using a Siemens model D 5000 diffractometer operating in Bragg−Brentano geometry. Adsorption/desorption isotherms were recorded using a Micromeritics ASAP 2010 instrument with nitrogen as adsorptive at −196 °C; the surface area was calculated according to the Brunauer−Emmett−Teller (BET) equation. Crystal size and shape surface analyses of nanoparticles were obtained by using the TEM (JEOL JEM-2100) and field-emission scanning electron microscope (FEI Magellan 400L instrument), respectively. The CO_2-TPD (TPD = temperature-programmed desorption) was performed to determine the basicity of MgO, CaO, and NiO catalysts using a ThermoFinnigan TPD/R/O 1100 Series instrument. Before adsorption, the sample was pretreated in He for 1 h (flow rate 50 cm^3/min) at the 450 °C at which MgO, CaO, and NiO were calcined. Then it was cooled to 100 °C and subsequently adsorbed by CO_2 for 1 h. The temperature-programmed desorption was carried out at a constant rate of 10 °C/min from ambient to 1000 °C.

Catalytic Test. NiO, CaO, MgO, and a physical mixture of NiO + CaO + MgO (equal NiO/CaO/MgO ratio) were used as catalysts for the steam gasification of toluene. Toluene was chosen as the model tar compound because it is one of the representative hydrocarbon compounds of the third group of the tar classification.[13] In addition, it is also a stable aromatic formed with a high-temperature gasification process. A schematic of the experimental setup is shown in Figure 1. The steam reforming of toluene was performed in a fixed-bed quartz reactor (inner diameter 10 mm) placed in a furnace in which the temperature is monitored. Water and toluene were introduced by syringe pumps into a vaporization furnace (250 °C) and then were transferred to the reactor by a flow containing a mixture of argon (carrier gas) and nitrogen (internal standard). The catalyst bed (500 mg) was supported by quartz wool, and a total flow of 3 L h^{-1} (gas hourly space velocity = 7500 h^{-1}) passes through it. The toluene concentration was fixed at 30 g N m^{-3} (0.8 vol % in the feed) in order to perform catalytic tests in more severe conditions in a biomass gasifier (up to 10 g N m^{-3}). The water concentration was fixed at the stoichiometric conditions (H_2O/C_7H_8 = 14/1). Toluene steam reforming has been performed in the presence of other gases (H_2, CO, CO_2, and CH_4) in concentrations similar to those measured in a biomass fluidized bed gasifier: 35 vol % of hydrogen, 30 vol % of carbon monoxide, 20 vol % of carbon dioxide, 12 vol % of methane, and 3 vol % of toluene (dry composition).[14,22] A set of two traps located at the reactor outlet was used to recover the nonconverted toluene fraction and/or heavy organic compounds in order to prevent condensation in the analysis lines. The gaseous effluent produced was analyzed continuously by gas chromatographs (Varian Instruments) equipped by flame-ionization detectors (FIDs) and thermal conductivity detectors (TCDs).

dx.doi.org/10.1021/sc300042e | ACS Sustainable Chem. Eng. 2013, 1, 80−86

RESULTS AND DISCUSSION

Catalyst Characterization. Single-crystalline CaO, MgO, and NiO were obtained through a calcination of $Ca(OH)_2$, $Mg(OH)_2$, and $Ni(OH)_2$ precursors, respectively. All precursors were produced isothermally by solvothermal processing at 170 °C. The XRD patterns of the products obtained after the precursors were calcined at 450 °C for 4 h are shown in Figure 2. As shown, the Bragg reflections are broad (Figure 2a),

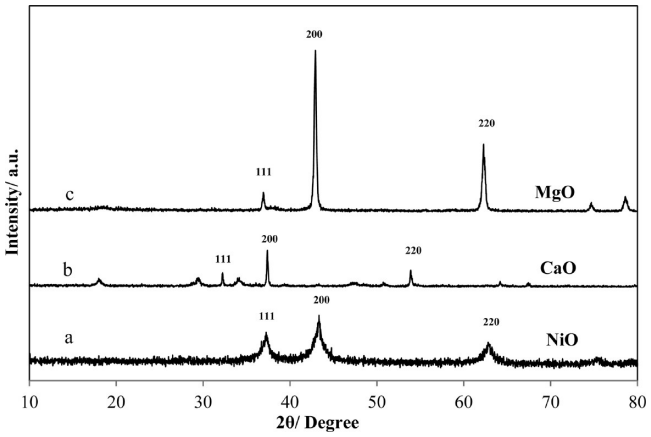

Figure 2. XRD patterns of pure CaO, MgO, and NiO.

indicating that NiO has a small size. No peaks from impurities are observed, indicating that the products were contained in the pure phase. All of the diffraction peaks in Figure 2a, not only the peak positions appearing at 2θ = 37.3, 43.3, and 62.9 but also their lattice parameters, were consistent with those of the standard spectrum of the pure, cubic NiO.[23,24] It was shown that these characteristic diffraction peaks in the pattern had a marked broadening effect. The results indicated that the products were NiO crystal of cubic structure having a high purity and small particle size with a fine crystal phase. According to the Scherrer formula[25] $D = 0.89\lambda/\beta\cos\theta$, where D represents the average particle size, β stands for the full width at half-height of the peaks, λ is the X-ray wavelength, and θ is the diffraction angle of the peak; the mean particle size of the product was calculated at 27.3 nm. These results are consistent with other research.[23,24]

XRD patterns of CaO (Figure 2b) and MgO (Figure 2c) are very sharp and intense and have no observed impurity peaks, indicating the complete formation of crystalline phase. Peak intensities reflect the total scattering from each plane in the phase's crystal structure and are directly dependent on the distribution of particular atoms in the structure. Thus, intensities are ultimately related to both structure and composition of the phase. The powder XRD pattern of the CaO (Figure 2b) shows the main characteristic peak of 111, 200, and 220, corresponding to 2θ values of 32.2, 37.3, and 53.8°, respectively. These patterns correspond to the face-centered cubic structure and are very close to the reported pattern.[26,27] For the MgO powder, the characteristic diffraction peaks corresponding to MgO crystalline were apparent at 2θ = 37.0, 43.0, 62.4, 74.8, and 78.7° (Figure 2c). These diffraction patterns were consistent with those of the standard spectrum of the pure and cubic MgO.[28−30]

The physical properties of the various catalysts are shown in Table 1. The crystallite sizes calculated using the Scherrer formula, based on the full width at half-maximum of the diffraction, are in agreement with BET surface area. The crystallite sizes were 58.1, 32.0, and 27.3 nm along the 200 planes for CaO, MgO, and NiO, respectively.

The SEM micrographs of the various nanoparticles are provided in Figure 3. The surface morphology and size of nanoparticles prepared by the solvothermal method can be well-controlled by temperature, reaction time, and reactants.[19−21] The size, the morphology, and their status of agglomeration of the as-synthesized nanoparticles were examined by TEM and are shown in Figure 4. From our research (Figure 4a), the SEM image of CaO powder was obtained showing monodispersed irregular spheres with a particle size distribution of 80−100 nm. From these images, it was obvious for the collected catalyst that its particles were of two types; one was a large particle in the shape of angular rock whereas the other appeared to be a cluster of thin plates.

As shown in Figures 3b and 4b, MgO has shown homogeneous morphologies and narrow size distributions. Figure 4b displays the cubic structure MgO. It is interesting to note that the estimated crystallite sizes are 32.0 and 27.5 nm for the 200 and 220 planes, respectively. Admittedly, direct comparison of the crystallite sizes from Scherrer estimation is less meaningful, considering the fact that particle dimension is not the only reason to account for the peak broadening. Here, the lattice distortion of MgO nanocrystallines is obviously significant. Figure 4c exhibits the TEM image of NiO, showing that shape and size of nanoparticle were maintained after the calcination of $Ni(OH)_2$. The diffraction pattern can be indexed to the face-centered cubic NiO, consistent with the XRD result.

Particle sizes based on TEM and XRD studies are also listed in Table 1 for the crystal and particle size comparisons. It was determined that the BET surface area values of all catalysts from this solvothermal method are generally much larger than the reported data for the salt-decomposition MgO, CaO, and NiO and fully comparable with the values for the sol−gel method.[31−33] It is noted that the particle sizes from TEM observation are systematically larger than corresponding XRD

Table 1. Textural and Physical-Chemical Properties of the CaO, MgO, and NiO Nanocrystallines

	fwhm[a](A°)			crystallite size[b] (nm)					
catalysts	111	200	220	111	200	220	particle size[c] (nm)	S_{BET}[d] ($m^2\ g^{-1}$)	CO_2 desorption[e] (unit area/g)
CaO	0.40	0.16	0.14	206.6	581.0	693.6	20	75.2	3.12
MgO	0.20	0.30	0.38	419.4	320.1	274.9	80	146.2	3.03
NiO	0.50	0.35	0.76	170.7	273.1	135.6	10	186.5	2.89
CaO/MgO/NiO								109.1	2.96

[a]Full width at half-maximum (fwhm) of 111, 200, and 220 reflections. [b]Crystallite size was calculated according to the Scherrer equation.[25] [c]Average particle sizes were estimated from TEM image. [d]Surface areas were obtained by BET method using adsorption data in p/p_0 range from 0.05 to 0.25. [e]Estimated from CO_2-TPD profiles.

dx.doi.org/10.1021/sc300042e | ACS Sustainable Chem. Eng. 2013, 1, 80−86

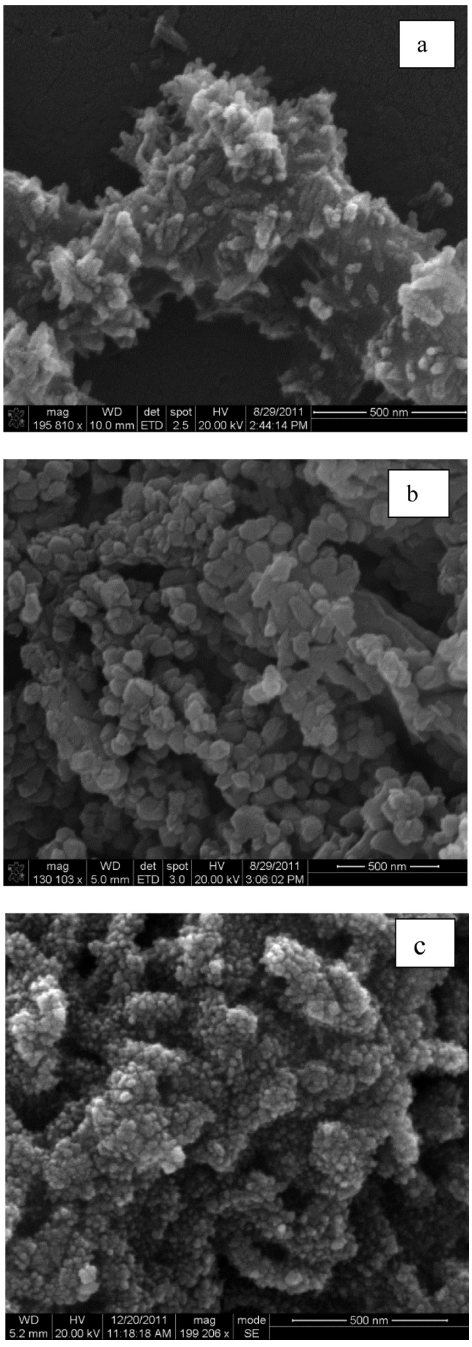

Figure 3. SEM image of CaO (a), MgO (b), and NiO (c) nanocrystallines.

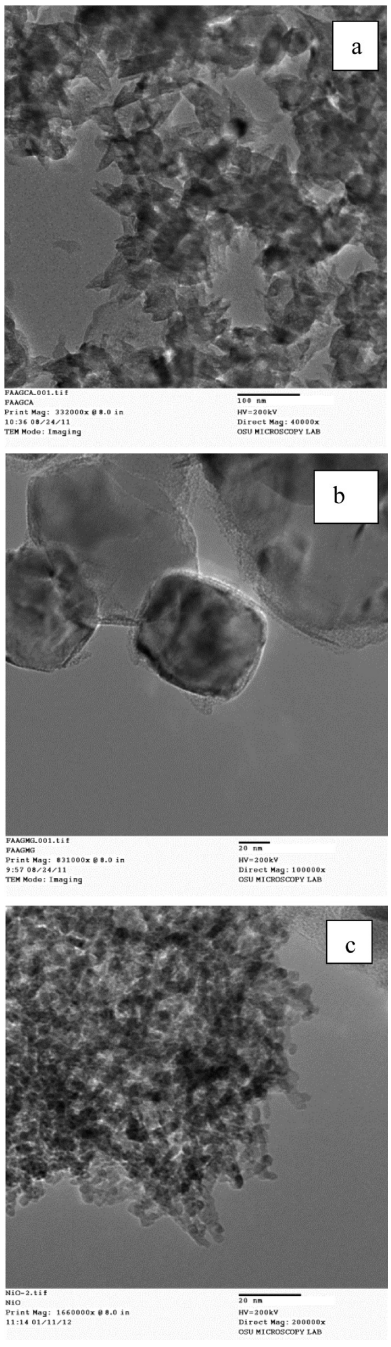

Figure 4. TEM image of CaO (a), MgO (b), and NiO (c) nanocrystallines.

values, meaning the observed lamella-like MgO, irregular CaO, and cubic NiO particles are actually composed of much smaller crystallites. It is a known fact that, during the calcination, water molecules are formed and lost between the two adjacent layers of hydroxyl ion, leaving a periclase structure with many defects and irregular intercrystallite channels.[34,35] These channels are likely the main cause of the high surface area feature of the MgO nanocrystallines. These channels can also be clearly seen in TEM images (Figure 3). Figure 4c shows a TEM micrograph of the NiO nanoparticle. It is shown that the NiO nanoparticles had spherical shapes, were well-dispersed with weak agglomeration, and had a narrow size distribution in a range from 5 to 8 nm. These observations are in good agreement with the result calculated by the Scherrer formula and the data of powder X-ray diffraction.

The specific surface area of the nanoparticles products calculated by the BET method after being measured by an ASAP 2010 instrument were 77.2, 146.2, and 186.5 $m^2\ g^{-1}$ for CaO, MgO, and NiO, respectively. Nanoparticles NiO and MgO are smaller in size and therefore gave the larger surface areas. The average crystallite size of NiO was determined to be 5 nm. In contract, CaO shows the lowest surface area because it has a relatively larger crystallite size at an average of 58 nm. It is well-known that the external surface of particles is used as a contact surface in catalytic reforming and gasification of biomass components. The larger the surface area of a catalyst, the higher is the likelihood of gas particles contacting these

dx.doi.org/10.1021/sc300042e | ACS Sustainable Chem. Eng. 2013, 1, 80−86

sites.[36−38] Finally, high surface area catalysts are expected to give high catalytic activity for a good gasification catalyst.

TPD experiments were performed with CO_2 as the probe molecule. TPD profiles of CO_2 desorbed in the temperature range of 100−1000 °C on MgO, CaO, and NiO are shown in Figure 5. The peaks in the TPD profiles are considered to

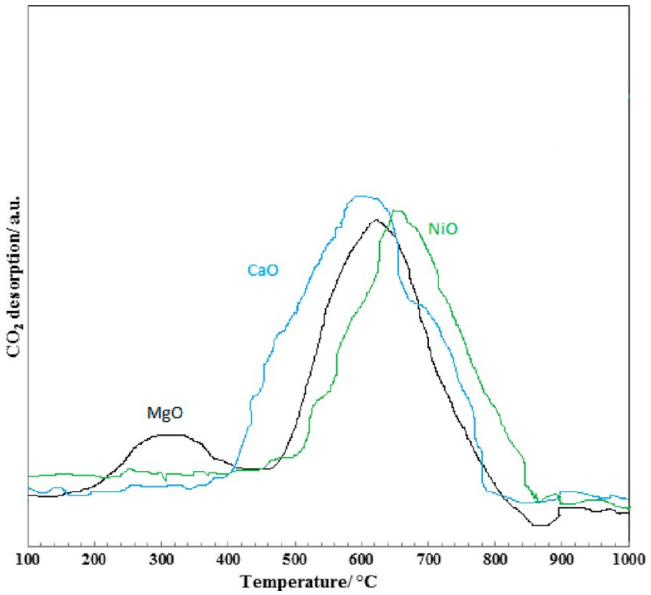

Figure 5. CO_2-TPD profiles of MgO, CaO, and NiO catalysts.

appear at higher temperatures as the basic sites on surfaces become stronger. The CO_2 desorption profiles consisted of two major peaks corresponding to different interactions of CO_2 with MgO surface sites. However, such peaks at lower temperatures were not observed for CaO and NiO, the reason for which is the absence of weak basic sites on surfaces CaO and NiO samples. From the peak positions, the base strength of the surfaces, measured by use of CO_2 as a probe, is in the following order: NiO > CaO > MgO. This order is in accordance with the order of the activities on the unit surface area basis.

For CO_2-TPD (Figure 5), MgO showed desorption peaks in the range of 200−400 and 450−850 °C, categorized into the weak and the strong basic sites, respectively. The basic quantity of CaO showed desorption peaks at 600 °C, accompanied by the shoulder peaks at around 450 and 700 °C. On the basis of the CO_2-TPD results, this demonstrated that CaO possessed only the medium-strength basic sites and base density. The base site of NiO was presented at 700 °C, accompanied by the shoulder peaks at around 550 °C. This indicated that NiO had strong base sites. The CaO sample showed a higher amount of medium basic sites compared to the NiO. The amounts of CO_2 desorption over each sample were calculated based on the area under the desorption peaks and are given Table 1. All samples showed strong basic sites, and the reaction data suggest that these sites are required for the reforming reaction.

Evaluation on the Catalytic Activity of Nanosized CaO, MgO, and NiO Particles in Toluene Reforming. To study the effect of reaction temperatures on toluene conversion (X_t) and selectivity to H_2 (Y_{H_2}), toluene steam reforming was performed over the CaO, MgO, and NiO catalysts in a temperature range of 500−800 °C for a substrate-to-catalyst ratio (S/C) = 2.1 and gas hourly space velocity (GHSV) of 7500 h^{-1}. Toluene conversion, H_2 yield, and CO_2 selectivity were compared over various catalysts at different reaction temperatures (Figures 6−8). CaO showed a slightly higher X_t than MgO, whereas NiO illustrated a significantly superior toluene conversion at all reaction temperatures. NiO is able to raise the catalytic toluene conversion of raw MgO plus CaO from below 50% up to 100% at 700 °C (Figure 6). Mean values for outlet concentrations of H_2, CO, CO_2, and CH_4 are shown in Table 2. It is clear that the mean hydrogen production is

Table 2. Mean Concentrations in the Outlet Gas for Toluene Steam Reforming by Catalyst; Reaction Temperature = 700 °C, GHSV = 7500 h^{-1}, and TOS = 7 h

			selectivity (%)		
catalyst	conversion[a] (%)	H_2 yield (%)	CO	CO_2	CH_4
MgO	42	46	81	19	
CaO	48	53	80	20	
NiO	94	74	63	37	<1
CaO/MgO/NiO	100	79	63	37	<1

[a] $X_t = [H_2]_{out}/18\cdot[C_7H_8]_{in}$.

proportional to toluene conversion and the CO_2/CO ratio. From the results, two temperature zones were distinguished. Below 700 °C, one can see toluene conversion and hydrogen yield enhanced quickly where the water gas shift reacton is

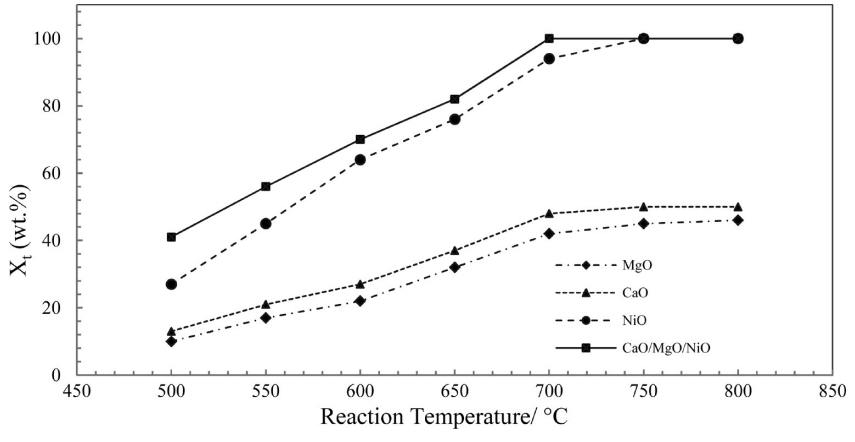

Figure 6. Toluene conversion on various catalysts (time on stream (TOS) = 7 h; S/C = 2.1; GHSV = 7500 h^{-1}).

dx.doi.org/10.1021/sc300042e | ACS Sustainable Chem. Eng. 2013, 1, 80−86

considered complete with increased reaction temperature. Toluene conversion and yield of H_2 were significantly enhanced with increased reaction temperature up to 700 °C (Figures 6 and 7). These rates slightly reduced above 700 °C due to the reverse water gas shift reaction, which is thermodynamically favorable at high temperatures. Trace CH_4 compound was observed in the products in addition to H_2, CO, and CO_2. Methane is probably a result of the cracking of toluene at lower reaction temperature. Above 750 °C, almost all toluene converted to H_2, CO, and CO_2 over NiO and mixed CaO/MgO/NiO catalyst. From Figure 7, mixed metal oxide (CaO/MgO/NiO) and NiO catalysts evaluated under the same process conditions produced higher H_2 yield than the CaO and MgO catalysts. The highest toluene conversion and H_2 selectivity was observed over mixed CaO/MgO/NiO catalyst. Basicity was higher for CaO catalyst as compared to mixed CaO/MgO/NiO catalyst but did not correlate with toluene conversion. In fact, a 100% conversion was reached with the mixed metal oxide versus 42%, 48%, and 94% for MgO, CaO, and NiO, respectively, which represents about 50% synergistic improvement. Deposition of carbonate compounds was observed on the bulk and mixed metal oxide catalysts. From Figure 8, it can be judged that different catalysts and reaction temperatures also had important influences on CO, CO_2 selectivity; the selectivity of CO_2 decreased by increasing temperature. CaO/MgO/NiO catalyst resulted in higher CO selectivity and nearly the same H_2 yield for the entire process.

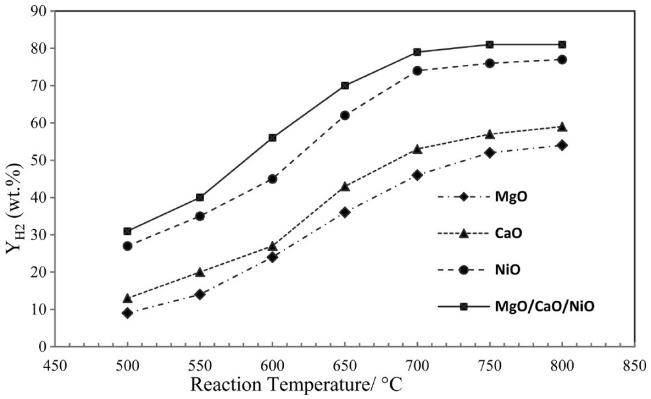

Figure 7. H_2 yield on various catalysts (TOS = 7 h; S/C = 2.1; GHSV = 7500 h^{-1}).

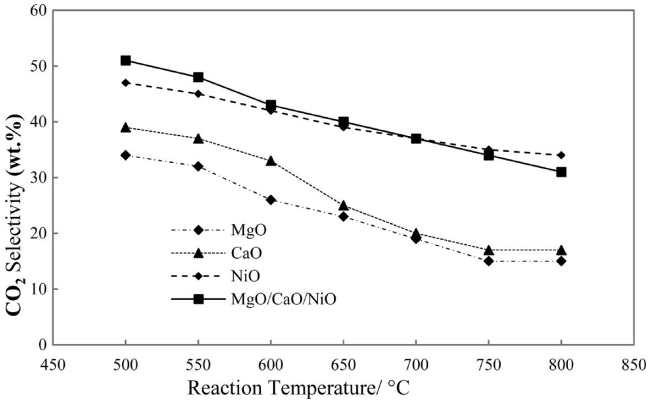

Figure 8. Selectivity of CO_2 on various catalysts (TOS = 7 h; S/C = 2.1; GHSV = 7500 h^{-1}).

Di Felice et al. have shown that the dissolution of NiO in the bulk CaO and MgO increases the exposed metal surface area of CaO/MgO/NiO catalyst.[39]

The optimized CaO/MgO/NiO catalyst was stable during 7 h of time on stream. The activity of mixed CaO/MgO/NiO catalyst confirmed the activity trends obtained by other researchers,[40] with the activity of dolomite (CaMgO) being higher than MgO or CaO activities due to the presence of more active sites in the array of Ca and/or Mg atoms. These results illustrate the importance of mixed metal oxides as effective catalysts during tar reforming. The efficiency of the CaO/MgO/NiO catalyst in tar removal from gasification gas was confirmed by steam reforming of toluene, a model tar compound. The importance of CaO/MgO/NiO catalyst was clearly demonstrated by the comparison with CaO, MgO, and NiO alone: higher activity, higher selectivity to H_2 and CO, and lower carbon deposition. The CaO/MgO/NiO mixture catalyst behaves more like NiO than MgO or CaO during reaction. It seems that some type of active site presents in NiO that is of a different nature than the sites that exist in either CaO or MgO catalysts. These differences may be responsible for the different activity and selectivity of the CaO/MgO/NiO mixture catalyst, being similar to those in NiO but somehow modified in strength or quantity by the presence of CaO or MgO catalysts. Methane compound was observed in the gas exiting from the reactor during toluene reforming over NiO and also CaO/MgO/NiO mixture catalysts; it clearly implys the differences between the active sites of NiO and also CaO/MgO/NiO mixture catalysts and those present in CaO or MgO catalysts. In conclusion, a good comparison between catalytic activity and H_2 selectivity was found for CaO/MgO/NiO mixture catalyst, demonstrating the efficiency improvement of reforming mixed metal oxide catalyst.

AUTHOR INFORMATION

Corresponding Author

*E-mail: ali.rownaghi@gmail.com; raymond.huhnke@okstate.edu. Phone: +1-405-744-5618. Fax: +1-405-744-6059.

Notes

The authors declare no competing financial interest.

ACKNOWLEDGMENTS

This work has been supported in part by the National Science Foundation EPSCoR program under Grant no. EPS 0814361 and the Director of the Oklahoma Agricultural Experiment Station.

REFERENCES

(1) Bozell, J. J. Feedstocks for the future—Biorefinery production of chemicals from renewable carbon. *Clean: Soil, Air, Water* **2008**, *36* (8), 641−647.

(2) Rownaghi, A. A.; Rezaei, F.; Hedlund, J. Yield of gasoline-range hydrocarbons as a function of uniform ZSM-5 crystal size. *Catal. Commun.* **2011**, *14* (1), 37−41.

(3) Rownaghi, A. A.; Hedlund, J. Methanol to gasoline-range hydrocarbons: Influence of nanocrystal size and mesoporosity on catalytic performance and product distribution of ZSM-5. *Ind. Eng. Chem. Res.* **2011**, *50*, 11872−11878.

(4) Torres, W.; Pansare, S. S.; Goodwin, J. G. Hot gas removal of tars, ammonia, and hydrogen sulfide from biomass gasification gas. *Catal. Rev.* **2007**, *49*, 407−456.

(5) Rownaghi, A. A.; Rezaei, F.; Hedlund, J. Uniform mesoporous ZSM-5 single crystals catalyst with high resistance to coke formation

for methanol deoxygenation. *Microporous and Mesoporous Mater.* **2012**, *151*, 26−33.
(6) Rownaghi, A. A.; Rezaei, F.; Stante, M.; Hedlund, J. Selective dehydration of methanol to dimethyl ether on ZSM-5 nanocrystals. *Appl. Catal., B* **2012**, *119*, 56−61.
(7) Carpenter, D. L.; Bain, R. L.; Davis, R. E.; Dutta, A.; Feik, C. J.; Gaston, K. R.; Jablonski, W.; Phillips, S. D.; Nimlos, M. R. Pilot-scale gasification of corn stover, switchgrass, wheat straw, and wood. 1. Parametric study and comparison with literature. *Ind. Eng. Chem. Res.* **2010**, *49*, 1856−1871.
(8) El-Rub, Z. A.; Bramer, E. A.; Brem, G. Evaluation of catalysts for tar elimination in biomass gasification processes. *Ind. Eng. Chem. Res.* **2004**, *43*, 6911−6919.
(9) Yung, M. M.; Jablonski, W. S.; Magrini-Bair, K. A. Review of catalytic conditioning of biomass-derived syngas. *Energy Fuels* **2009**, *23*, 1874−1887.
(10) Gerber, M. A. *Review of Novel Catalysts for Biomass Tar Cracking and Methane Reforming*. PNNL-16950; Prepared for the U.S. Department of Energy DE-AC05-76RL01830, October 2007.
(11) Neeft, J. P. A.; Knoef, H. A. M.; Onaji, P. *Behavior of tar in biomass gasification systems. Tar related problems and their solutions*. November Report No. 9919. Energy from Waste and Biomass (EWAB), The Netherlands, 1999.
(12) Rownaghi, A. A.; Rezaei, F.; Hedlund, J. Selective formation of light olefin by *n*-hexane cracking over HZSM-5: Influence of crystal size and acid sites of nano- and micrometer-sized crystals. *Chem. Eng. J.* **2012**, *191*, 528−533.
(13) Milne, T. A.; Abatzoglou, N.; Evans, R. J.. *Biomass Gasifier-Tars*; National Renewable Energy Laboratory Technical Report NREL/TP 570-25357; National Renewable Energy Laboratory: Golden, CO, 1998.
(14) Dayton, D. *A Review of the Literature on Catalytic Biomass Tar Destruction*; National Renewable Energy Laboratory Technical Report NREL/TP-510-32815; National Renewable Energy Laboratory: Golden, CO, 2002.
(15) Ngamcharussrivichai, C.; Nunthasanti, P.; Tanachai, S.; Bunyakiat, K. Biodiesel production through transesterification over natural calciums. *Fuel Process. Technol.* **2010**, *91*, 1409−1415.
(16) Ngamcharussrivichai, C.; Wiwatnimit, W.; Wangnoi, S. The catalyst modified from dolomite calcined at 600 and 700°C. *J. Mol. Catal. A: Chem.* **2007**, *276*, 24−33.
(17) Magrini-Bair, K. A.; Czernik, S.; French, R.; Parent, Y. O.; Chornet, E.; Dayton, D. C.; Feik, C.; Bain, R. Fluidizable reforming catalyst development of conditioning biomass-derived syngas. *Appl. Catal., A* **2007**, *318*, 199−206.
(18) Vollath, D. Nanomaterials: An Introduction to Synthesis, Properties and Application; Wiley-VCH Verlag GmbH&Co. KGaA: Weinheim, Germany, 2008.
(19) Rownaghi, A. A.; Taufiq-Yap, Y. H.; Rezaei, F. Solvothermal synthesis of vanadium phosphate catalysts for *n*-butane oxidation. *Chem. Eng. J.* **2009**, *155*, 514−522.
(20) Rownaghi, A. A.; Taufiq-Yap, Y. H.; Rezaei, F. Innovative process for the synthesis of vanadyl pyrophosphate as a highly selective catalyst for *n*-butane oxidation. *Chem. Eng. J.* **2010**, *165*, 328−335.
(21) Rownaghi, A. A.; Taufiq-Yap, Y. H. Novel synthesis techniques for preparation of ultrahigh-crystalline vanadyl pyrophosphate as a highly selective catalyst for *n*-butane oxidation. *Ind. Eng. Chem. Res.* **2010**, *49*, 2135−2143.
(22) Virginiea, M.; Coursona, C.; Niznanskyb, D.; Chaouic, N.; Kiennemanna, A. Characterization and reactivity in toluene reforming of a Fe/olivine catalyst designed for gas cleanup in biomass gasification. *Appl.Catal., B* **2010**, *101*, 90−100.
(23) Liu, X. M.; Zhang, X. G.; Fu, S. Y. Preparation of urchinlike NiO nanostructures and their electrochemical capacitive behaviors. *Mater. Res. Bull.* **2006**, *41*, 620−627.
(24) Li, G. J.; Huang, X. X.; Shi, Y.; Guo, J. K. Preparation and characteristics of nanocrystalline NiO by organic solvent method. *Mater. Lett.* **2001**, *51*, 325−330.
(25) Patterson, A. L. The Scherrer formula for X-ray particle size determination. *Phys. Rev.* **1939**, *56*, 978−982.
(26) Liu, W.; Low, N. W. L.; Feng, B.; Wang, G.; Diniz da Costa, J. C. Calcium precursors for the production of CaO sorbents for multicycle CO_2 capture. *Environ. Sci. Technol.* **2010**, *44*, 841−847.
(27) Martínez, S. L.; Romero, R.; Lopez, J. C.; Romero, A.; Mendieta, V. S.; Natividad, R. Preparation and characterization of CaO nanoparticles/NaX zeolite caralysts for the transesterification of sunflower oil. *Ind. Eng. Chem. Res.* **2011**, *50*, 2665−2670.
(28) Aramendia, M. A.; Betez, J. A.; Borau, V.; Jimnez, C.; Marinas, J. M.; Ruiz, J. R.; Urbano, F. Characterization of various magnesium oxides by XRD and ^{1}H MAS NMR spectroscopy. *J. Solid State Chem.* **1999**, *144*, 25−29.
(29) Aramendia, M. A.; Betez, J. A.; Borau, V.; Jimnez, C.; Marinas, J. M.; Ruiz, J. R.; Urbano, F. Preparation of Pt/MgO catalysts. Influence of the precursor metal salt and solvent used. *Colloids Surf.* **2000**, *168*, 27−33.
(30) Wu, X. F.; Hu, G. S.; Wang, B. B.; Yang, Y. Y. Synthesis and characterization of superfine magnesium hydroxide with monodispersity. *J. Cryst. Growth* **2008**, *310*, 457−461.
(31) Florin, N. H.; Harris, A. T. Reactivity of CaO derived from nano-sized $CaCO_3$ particles through multiple CO_2 capture and release cycles. *Chem. Eng. Sci.* **2009**, *64*, 187−191.
(32) Wang, J. A.; Novaro, O.; Bokhimi, X.; Lopez, T.; Gomez, R.; Navarrete, J.; Llanos, M. E.; Lopez-Salinas, E. Preparation of Pd−Pt bimetallic colloids with controllable core/shell structures. *J. Phys. Chem. B* **1997**, *101*, 7448.
(33) Wang, J. A.; Novaro, O.; Bokhimi, X.; Lopez, T.; Gomez, R.; Navarrete, J.; Llanos, M. E.; Lopez-Salinas, E. Characterizations of the thermal decomposition of brucite prepared by sol−gel technique for synthesis of nanocrystalline MgO. *Mater. Lett.* **1998**, *35*, 317−323.
(34) Li, Q.; Wang, L.-S.; Hu, B.-Y.; Yang, C.; Zhou, L.; Zhang, L. Preparation and characterization of NiO nanoparticles through calcination of malate gel. *Mater. Lett.* **2007**, *6*, 1615−1618.
(35) Gesser, H. D.; Goswami, P. C. Aerogels and related porous materials. *Chem. Rev.* **1989**, *89*, 765−788.
(36) Taralas, G.; Kontominas, M. G. Tar elimination and hot-gas conditioning in thermochemical conversion. *Fuel* **2004**, *83*, 1235−1245.
(37) Swierczynski, D.; Libs, S.; Courson, C.; Kiennemann, A. Steam reforming of tar from a biomass gasification process over Ni/olivine catalyst using toluene as a model compound. *Appl. Catal., B* **2007**, *74*, 211−222.
(38) Li, J.; Yan, R.; Xiao, B.; Liang, D. T.; Du, L. Development of nano-NiO/Al_2O_3 catalyst to be used for tar removal in biomass gasification. *Environ. Sci. Technol.* **2008**, *42*, 6224−6229.
(39) Di Felice, L.; Courson, C.; Foscolo, P. U.; Kiennemann, A. Iron and nickel doped alkaline-earth catalysts for biomass gasification with simultaneous tar reformation and CO_2 capture. *Int. J. Hydrogen Energy* **2011**, *36*, 5296−5310.
(40) Li, C.; Hirabayashi, D.; Suzuki, K. Steam reforming of biomass tar producing H_2-rich gases over $Ni/MgO_x/CaO_{1-x}$ catalyst. *Bioresour. Technol.* **2010**, *101*, S97−S100.